Journal of Medicinal Chemistry

Article

pubs.acs.org/jmc

Controlling the Dissociation of Ligands from the Adenosine A_{2A} Receptor through Modulation of Salt Bridge Strength

Elena Segala,[†,#] Dong Guo,[‡,#] Robert K. Y. Cheng,[†,#] Andrea Bortolato,[†] Francesca Deflorian,[†] Andrew S. Doré,[†] James C. Errey,[†] Laura H. Heitman,[‡] Adriaan P. IJzerman,[‡] Fiona H. Marshall,[†] and Robert M. Cooke*[,†]

[†]Heptares Therapeutics Ltd, Biopark Broadwater Road, Welwyn Garden City AL7 3AX, U.K.

[‡]Division of Medicinal Chemistry, Leiden Academic Centre for Drug Research (LACDR), Leiden University P.O. Box 9502, 2300 RA Leiden, the Netherlands

Supporting Information

ABSTRACT: The association and dissociation kinetics of ligands binding to proteins vary considerably, but the mechanisms behind this variability are poorly understood, limiting their utilization for drug discovery. This is particularly so for G protein-coupled receptors (GPCRs) where high resolution structural information is only beginning to emerge. Engineering the human A_{2A} adenosine receptor has allowed structures to be solved in complex with the reference compound ZM241385 and four related ligands at high resolution. Differences between the structures are limited, with the most pronounced being the interaction of each ligand with a salt bridge on the extracellular side of the receptor. Mutagenesis experiments confirm the role of this salt bridge in controlling the dissociation kinetics of the ligands from the receptor, while molecular dynamics simulations demonstrate the ability of ligands to modulate salt bridge stability. These results shed light on a structural determinant of ligand dissociation kinetics and identify a means by which this property may be optimized.

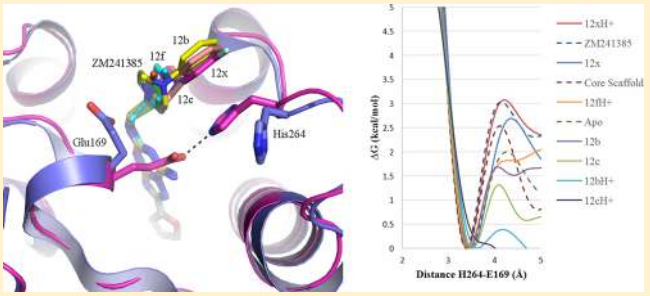

INTRODUCTION

G protein-coupled receptors (GPCRs) comprise the largest family of cell surface receptors in eukaryotes and are the targets for approximately one-third of all marketed drugs.[1] Recent advances in GPCR structural biology have enabled the visualization of ligand−receptor interactions at an atomic level, dramatically boosting the impact of structure-based approaches in drug discovery.[2] As has been done for soluble proteins for many years, X-ray structures of GPCRs are now being used to identify new binding sites for ligands and highlight means by which their affinities can be improved while retaining drug-like properties.

Far less advanced is the use of structural information to understand the association and dissociation rates of ligands to proteins. The ligand−receptor residence time, defined as the reciprocal of the dissociation rate constant, is a topic of increasing interest in drug discovery.[3] Considering binding kinetics in the selection of candidate drug molecules could potentially lead to therapies with improved clinical efficacy or safety profiles.[4] Molecular features that could influence binding kinetics have been identified,[5] but thus far there has been little use of structural information to guide the optimization of ligand−receptor residence times. This is due in part to ligand optimization efforts being typically driven by binding affinities rather than rate constants but is more due to a paucity of examples where interactions determining dissociation kinetics are well understood and can be altered by ligand design.

The A_{2A} adenosine receptor (A_{2A}R) is a promising target for a range of diseases, including ADHD (attention deficit hyperactivity disorder) and Parkinson's, and is the target of one approved antagonist drug, istradefylline, with ongoing efforts to discover other small molecules with differentiated properties.[6] Antagonism of A_{2A}R has also generated considerable interest as an immunotherapeutic treatment for cancer,[7] with the relatively high levels of adenosine in the tumor microenvironment providing validation for the concept and suggesting that prolonged receptor blockade through an increased residence time would be beneficial. A recent study of human A_{2A}R[8] highlighted a number of features of the receptor that influence the dissociation of the well-established tool antagonist ZM241385. This includes a salt bridge formed by Glu169 in the second extracellular loop of the receptor, between transmembrane helices 4 and 5, and His264 in the third extracellular loop, between helices 6 and 7. Here we report the X-ray structures of a series of ligands related to and including ZM241385, bound to a thermostabilized human A_{2A}R. These ligands (Figure 1) have previously been shown to

Received: April 27, 2016
Published: June 17, 2016

DOI: 10.1021/acs.jmedchem.6b00653
J. Med. Chem. 2016, 59, 6470−6479

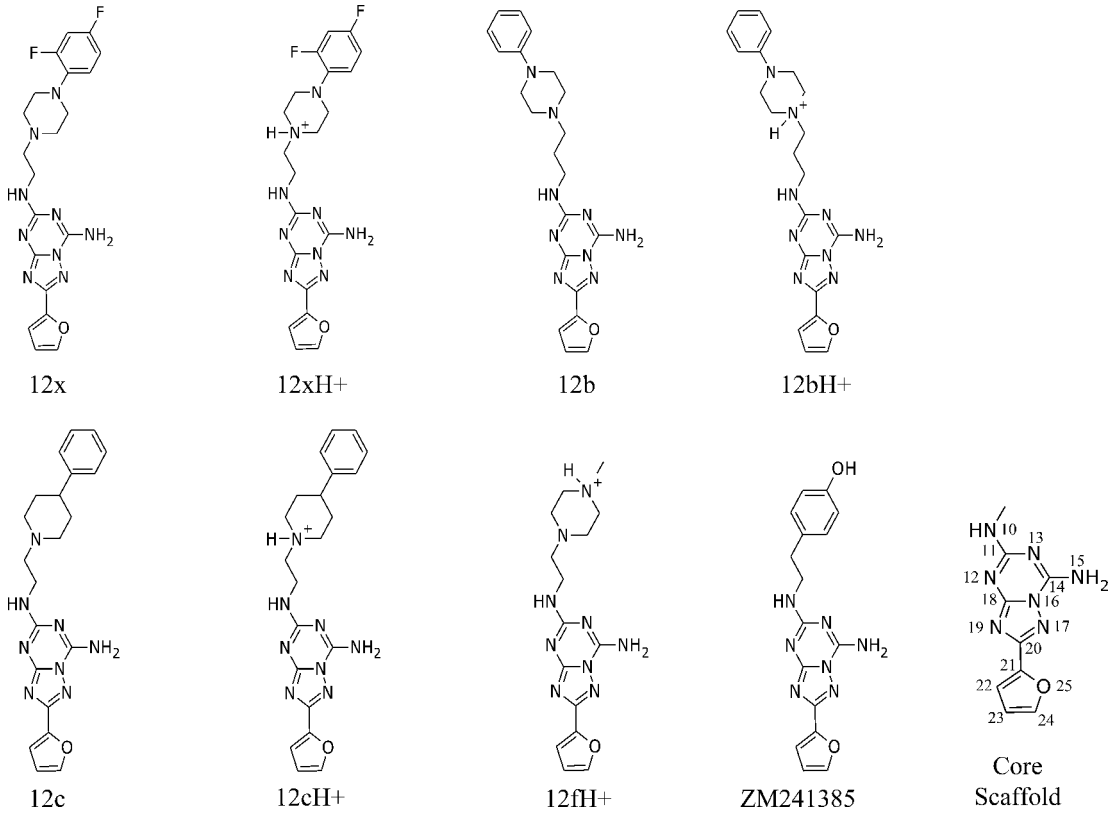

Figure 1. Ligands used in this study: **12x**, **12b**, **12c**, **12f**, and ZM241385. The core scaffold represents the common part of all ligands, with the atom numbering based on ZM241385. Ligands **12x**, **12b**, and **12c** are represented in both the neutral and the protonated states, because both could exist and were considered in the metadynamics studies. For **12f**, only the protonated state was predicted to exist.

Table 1. Affinity and Kinetics of ZM241385, 12x, 12c, 12b, and 12f for the A_{2A}-StaR2-bRIL and the A_{2A}R-WT Constructs[a]

	K_i (nM)		k_{on} ($M^{-1}\cdot min^{-1}$)		k_{off} (min^{-1})		RT (min)	
compd	A_{2A}-StaR2-bRIL	A_{2A}R-WT[b]	A_{2A}-StaR2-bRIL	A_{2A}R-WT[b]	A_{2A}-StaR2-bRIL	A_{2A}R-WT[b]	A_{2A}-StaR2-bRIL	A_{2A}R-WT[b]
ZM241385	0.53 ± 0.003	0.40 ± 0.03	(2.1 ± 0.3) × 10^7	(1.3 ± 0.3) × 10^8	0.0027 ± 0.0001	0.014 ± 0.003	370 ± 14	71 ± 21
12x	0.35 ± 0.02	0.33 ± 0.04	(6.0 ± 0.4) × 10^6	(3.4 ± 0.4) × 10^7	0.0029 ± 0.0004	0.0031 ± 0.0002	344 ± 47	323 ± 25
12c	1.1 ± 0.0	3.8 ± 0.8	(1.6 ± 0.3) × 10^7	(2.0 ± 1.0) × 10^8	0.024 ± 0.002	0.35 ± 0.03	42 ± 4	3 ± 1
12b	1.5 ± 0.1	1.3 ± 0.1	(7.8 ± 1.4) × 10^6	(1.6 ± 0.6) × 10^8	0.021 ± 0.001	0.25 ± 0.01	50 ± 3	4 ± 1
12f	18 ± 2	31 ± 6	(2.4 ± 0.2) × 10^6	(5.7 ± 2.0) × 10^6	0.098 ± 0.005	0.25 ± 0.10	10 ± 1	4 ± 1

[a]Data are mean ± SEM from at least three independent experiments each performed in duplicate. [b]Values from ref 9.

have high affinities for the human A_{2A}R but with a 100-fold range of dissociation rate constants.[9] The elucidation of high resolution X-ray structures of these ligands complexed with A_{2A}R highlights differences in the interactions between the ligands and the Glu169−His264 salt bridge, which may contribute to the variation in dissociation kinetics. Mutation of either residue to disrupt the salt bridge increases the dissociation rate for long residence time ligands, while the residence time for ligands correlates with the energy required to break the salt bridge as estimated *in silico* using a metadynamics[10] protocol. Long residence time ligands appear to stabilize the Glu−His ionic interaction, while fast off-rate derivatives were generally predicted to destabilize this salt bridge. These high resolution structures thus highlight a key determinant of ligand−receptor residence time for the human A_{2A}R and identify a mechanism by which this can be optimized in kinetics-directed drug design.

RESULTS

Characterization of the A_{2A}-StaR2-bRIL. The binding affinities and kinetics were determined for five ligands of A_{2A}-StaR2-bRIL, which consists of human A_{2A}R with mutations at A54L$^{2.52}$, T88A$^{3.36}$, R107A$^{3.55}$, K122A$^{4.43}$, N154A, L202A$^{5.63}$, L235A$^{6.37}$, V239A$^{6.41}$, and S277A$^{7.42}$ (the superscript refers to Ballesteros−Weinstein numbering for residues in transmembrane helices[11]) used in previous studies,[12] with the addition of a thermostabilized apocytochrome b 562 (bRIL)[13] within a truncated third intracellular loop. The affinities and kinetics of ligands ZM241385, **12x**,[9] **12c**,[9] **12b**,[9] and **12f**[9] (Figure 1) binding to the A_{2A}-StaR2-bRIL were extensively characterized and compared with those for binding to the A_{2A}R-WT (wild-type) construct (Table 1). Antagonist [^{3}H]-ZM241385 radioligand displacement assays showed that the five ligands have binding affinities for the A_{2A}-StaR2-bRIL between 0.35 nM (ZM241385) and 18 nM (**12f**). These values are in general agreement with the binding affinities measured for A_{2A}R-WT. The relative residence times are also in general agreement

DOI: 10.1021/acs.jmedchem.6b00653
J. Med. Chem. 2016, 59, 6470−6479

Table 2. X-ray Data Collection and Refinement Statistics for A_{2A}-StaR2-bRIL in Complex with Ligands

	ZM241385	12x	12b	12c	12f
			Data Collection		
Number of crystals	21	7	3	1	3
Space group	$C222_1$	$C222_1$	$C222_1$	$C222_1$	$C222_1$
cell dimensions					
a, *b*, *c* (Å)	39.62, 180.80, 140.25	39.38, 180.34, 140.86	39.53, 181.26, 140.92	39.38, 180.04, 139.84	39.28, 179.70, 140.14
α, *β*, *γ* (deg)	90.00, 90.00, 90.00	90.00, 90.00, 90.00	90.00, 90.00, 90.00	90.00, 90.00, 90.00	90.00, 90.00, 90.00
resolution[a] (Å)	33.73−1.72 (1.75−1.72)	33.62−2.1 (2.16−2.1)	33.82−2.20 (2.27−2.2)	33.71−1.90 (1.94−1.90)	33.67−2.00 (2.05−2.00)
R_{sym} (R_{merge})	0.111 (0.994)	0.147 (0.959)	0.189 (0.888)	0.103 (1.007)	0.170 (1.185)
I (σI)	7.2 (1.5)	9.0 (1.5)	6.7 (1.6)	10.0 (1.5)	10.7 (1.9)
completeness (%)	93.3 (93.5)	94.4 (77.7)	94.6 (78.0)	99.4 (99.8)	99.7 (99.8)
redundancy	3.1 (3.0)	5.0 (1.8)	3.2 (2.6)	4.4 (4.4)	8.0 (8.2)
			Refinement		
resolution (Å)	1.72	2.1	2.2	1.9	2.0
no. reflns	94804	27587	46339	75271	33945
R_{work}/R_{free}	0.166/0.200	0.189/0.219	0.198/0.234	0.167/0.201	0.175/0.201
no. atoms					
protein	3171	3154	3153	3234	3131
ligand	25	32	31	30	25
Na	1	1	1	1	1
cholesterol	112	56	84	112	84
lipids	383	322	398	407	410
water	176	96	133	162	166
other					10
B-factors					
protein	34.13	48.62	33.08	36.37	33.43
ligand	17.09	26.12	30.99	23.64	23.38
Na	31.86	52.25	35.39	29.29	33.37
cholesterol	46.71	33.90	31.55	45.6	30.79
lipids	55.67	63.84	54.83	58.52	58.59
water	40.6	67.97	34.15	40.72	38.41
other					33.88
rms deviations					
bond lengths (Å)	0.01	0.003	0.004	0.015	0.003
bond angles (deg)	1.314	1.014	1.052	1.575	1.012
Ramachandran plot statistics[b] (%)					
favored regions	99.5	99.25	99.0	99.27	99.5
allowed regions	0.5	0.75	1.0	0.73	0.5
disallowed regions	0	0	0	0	0

[a]Values in parentheses are for highest-resolution shell. [b]As defined in MolProbity.[31]

between the two forms of the receptor; however, with the exception of **12x**, each ligand displayed a longer residence time at the A_{2A}-StaR2-bRIL compared with that at the A_{2A}R-WT. Hence for the A_{2A}R-WT the residence time of ZM241385 is intermediate between those of **12x** (longer) and **12b**, **12c**, and **12f** (shorter), while for the A_{2A}-StaR2-bRIL ZM241385 and **12x** have similar residence times, both being longer than those of **12b**, **12c**, and **12f** (Table 1).

Comparisons between the Structures of the Five A_{2A}R ligands and Previous Structures of ZM241385. The A_{2A}-StaR2-bRIL protein crystallized with each of the five tool ligands in spacegroup $C222_1$ with one A_{2A}-StaR2-bRIL molecule per asymmetric unit. Data collection and refinement statistics for the five structures are given in Table 2. Consistent with the presence of the same furan-substituted triazolotriazine core in each of the five ligands used in this study, the structures of all five complexes in this region (Figure 2) are nearly identical (no differences greater than experimental error). For each ligand, the core sits on one side of a cavity formed by the transmembrane helices, which contains a network of water molecules stretching almost the full transmembrane length of the receptor, and a sodium ion in the position previously reported.[13] The furan ring of each ligand is furthest from the extracellular surface, with the oxygen located 3.1 Å from the δN of Asn253$^{6.55}$, consistent with a weak interaction. The torsion angles between the planes of the furan and the triazolotriazine rings are all 15°.

The triazolotriazine rings are sandwiched between two hydrophobic surfaces, formed by the aromatic ring of Phe168 on one side and Leu249$^{6.51}$, Ile274$^{7.39}$, and Met270$^{7.35}$ on the other (Figure 2A). One edge of the triazolotriazine core is directed toward the water filled cavity of the receptor, with water molecules located at 2.9 and 2.8 Å from ring atoms N12 and N19, respectively. On the other edge, the exocyclic primary

DOI: 10.1021/acs.jmedchem.6b00653
J. Med. Chem. 2016, 59, 6470−6479

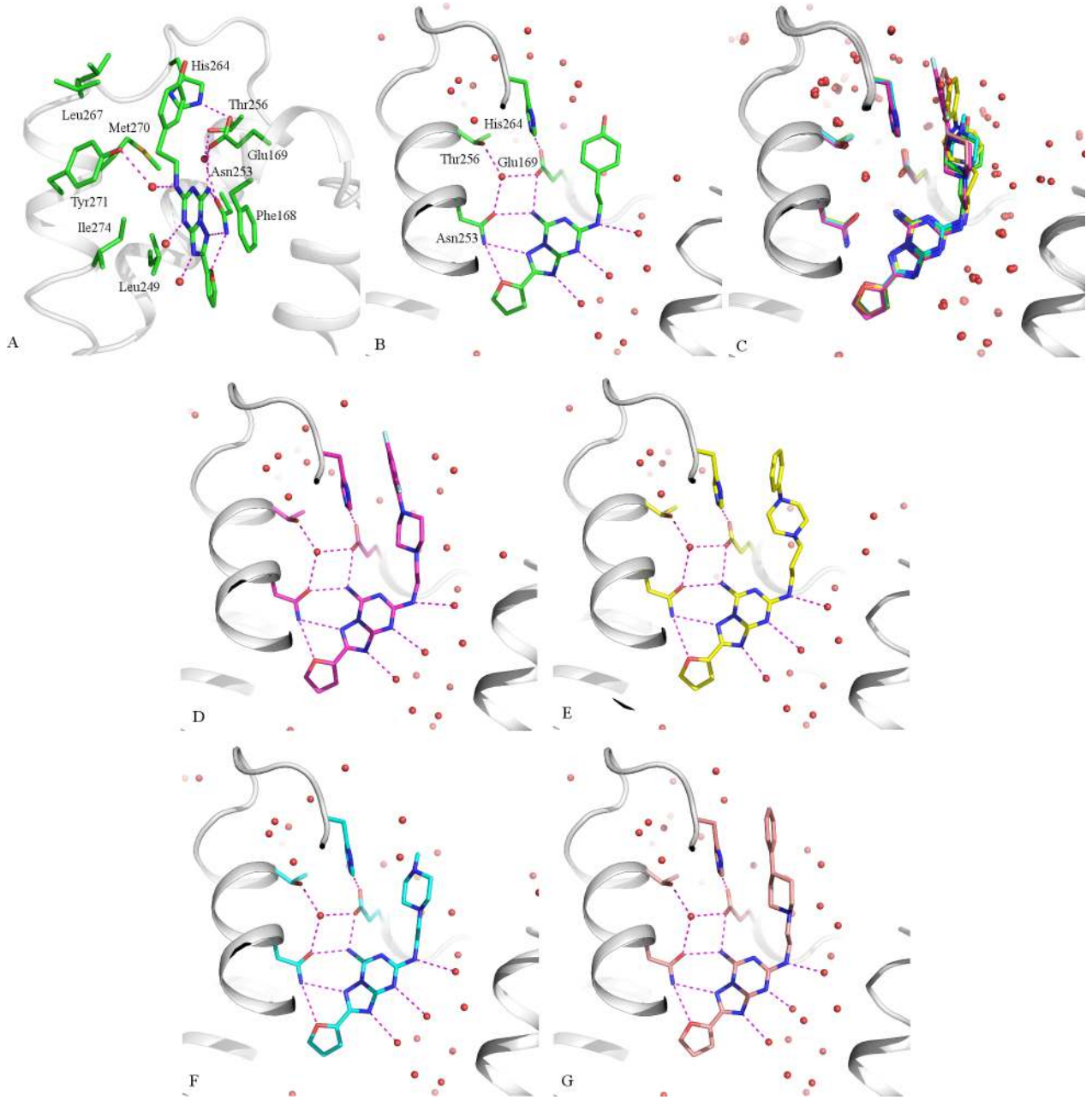

Figure 2. View of the five antagonists in the binding site of the A_{2A}-StaR2-bRIL: (A, B) ZM241385, (C) superposition of the binding sites of ZM241385, **12x**, **12b**, **12f**, and **12c**, (D) **12x**, (E) **12b**, (F) **12f**, and (G) **12c**. Water molecules are shown as red spheres and hydrogen bonds as red lines.

amine (N15) H bonds with side chain oxygen atoms of Asn253$^{6.55}$ and Glu169; these are also bridged by a water molecule, which forms an additional H-bond to the side chain of Thr256$^{6.58}$. The exocyclic secondary amine (N10) is also bridged to the phenolic oxygen of Tyr271$^{7.35}$ by a water molecule. Beyond N10, the substituents of the different ligands structurally diverge but are all directed toward the extracellular surface, sitting between residues Tyr271$^{7.35}$ and Leu267 on one side and a salt bridge formed by Glu169 and His264 on the other (Figure 2A). The differences in the conformation of the protein backbone and side chains are minimal, with only slight variations in side chain positions observed for Leu267 and Tyr271$^{7.35}$.

Although His264 and Glu169 are similarly positioned in each of the five structures, notable differences are apparent in how the ligands interact with these residues (Figure 3). In the case of ZM241385, the phenolic substituent lies edge-on to the salt bridge, with the closest phenolic carbon atom approximately 3.8 Å from the His ring. In **12f**, the phenol of ZM241385 is replaced with an N-linked piperazine ring, which sits in the same general region but is nonplanar. The structure with **12x**, in which a difluorophenyl group is attached to the other nitrogen of the piperazine, shows a 1.0 Å shift of the previously terminal piperazine nitrogen, with the difluorophenyl group approximately 3.6 Å from the ring of His264 in a π-stacking arrangement. The piperidine ring of **12c** superimposes with the piperazine ring of **12x**, but the phenyl headgroup is twisted slightly away from His264 compared with the difluorophenyl headgroup of **12x**. The piperazine of **12b** is attached to the triazolotriazine core by a three carbon link and does not

DOI: 10.1021/acs.jmedchem.6b00653
J. Med. Chem. 2016, 59, 6470−6479

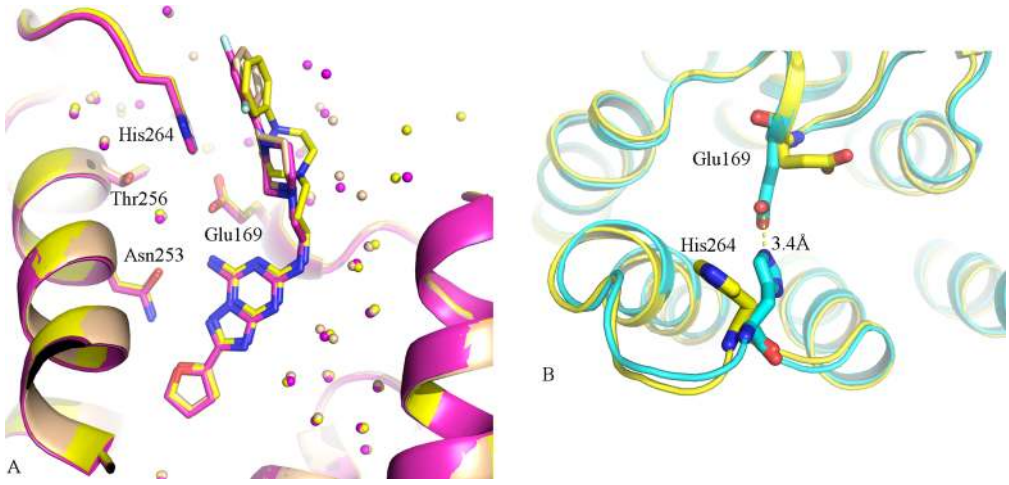

Figure 3. (A) Superposition of the ligand binding site in the crystal structure of the A_{2A}-StaR2-bRIL in complex with **12x** (magenta), **12b** (brown), and **12c** (yellow). (B) Difference in the orthosteric site accessibility between the A_{2A}R crystal structures with the salt bridge formed (in cyan, structure from this study) and broken (in yellow from PDB ID 3PWH[12]).

superimpose with the piperazine or piperidine rings of **12x**, **12c**, and **12f**. The phenyl ring of **12b** does approach similar locations to those of **12x** and **12c**, but this requires an axial conformation from the piperazine ring, and the phenyl group is swung away from the His264 imidazole ring by approximately 1.2 Å.

The overall A_{2A}-StaR2-bRIL structure in complex with ZM241385 superimposes well with the 2.6 Å resolution crystal structure of the A_{2A}R−T4L fusion protein with ZM241385 (PDB ID 3EML),[14] with an RMSD of 0.91 Å for 270 equivalent Cα atoms, and the more recent 1.8 Å resolution A_{2A}R-bRIL fusion protein with ZM241385 (PDB ID 4EIY),[13] with an RMSD of 0.32 Å for 290 equivalent Cα atoms. The structure is somewhat different from the previously reported thermostabilized nonfused A_{2A}R structure with ZM241385 (PDB ID 3PWH)[12] obtained at higher pH, in which the Glu169−His264 salt bridge is not present, the conformation of the extracellular loops is altered, and the phenol group of ZM241385 is differently oriented.

Effect of the Salt Bridge on Ligand Dissociation Kinetics and Effect of the Ligands on Salt Bridge Stability. The role of the Glu169−His264 salt bridge in modulating the kinetics of ligand binding was investigated in a radioligand washout experiment using A_{2A}R-WT. The receptor was incubated with compounds, washed three times to remove any unbound ligand, and then incubated with [^{3}H]-ZM241385 to label any free receptor not occupied by the unlabeled ligands. Preincubation with ZM241385 or **12c**, followed by washing, allowed complete labeling with [^{3}H]-ZM241385, whereas preincubation with **12x** followed by washing resulted in only partial labeling (Table 3), consistent with the relative residence times of the ligands. Disrupting the salt bridge by mutating either His264 or Glu169 caused an increase in labeling following preincubation and wash out with **12x**, but not with ZM241385 or **12c** (Table 3).

The energy required to break the Glu169−His264 salt bridge was estimated using a metadynamics protocol.[10] The free energy surface representing the salt bridge was defined using the distance between the histidine ring and the glutamic acid and the Cα, Cβ dihedral angle of the histidine. During the simulation, the free energy landscape of the salt bridge was altered, based on previously sampled conformations, to prevent the system returning to the low energy state with the salt bridge intact. The stability of the salt bridge was estimated from the energy required to be added to break the bridge and allow the two amino acids to assume the rotameric states observed in the high pH crystal form (PDB ID 3PWH)[12] (Figure 3B).

Table 3. Level of Binding to [^{3}H]-ZM241385 after Preincubation of HEK293 Cell Membranes Expressing the A_{2A}R-WT, -His264A, or -Glu169Q with 12x, 12c, and ZM241385 (1 μM)[a]

compd	A_{2A}R-WT (%)	His264A (%)	Glu169Q (%)
12x	76 ± 5	97 ± 5	102 ± 7*
12c	105 ± 3	105 ± 10	105 ± 3
ZM241385	105 ± 2	106 ± 14	97 ± 4

[a]Data are mean ± SEM from at least three independent experiments each performed in duplicate. Significantly different from wild-type with *p < 0.05 (one-way ANOVA with Dunnett's test).

To estimate the stability of the salt bridge in the absence of any ligand, the same metadynamics protocol was used on the apo protein, and we also evaluated the core scaffold, common among the ligands (Figure 1). Simulations were performed for each of the five ligands for which X-ray structures were obtained. For **12x**, **12b**, and **12c**, it was not certain whether the neutral or protonated form would be present, and both forms were evaluated (Figure 1).

In the absence of any ligand bound, the salt bridge stability was estimated to be 2 kcal/mol (Figure 4). The core scaffold increases its strength by about 0.5 kcal/mol. The longer receptor residence time ligands ZM241385 and **12x** (both in the neutral and positively charged forms) further stabilized this interaction to 2.7−3.1 kcal/mol. The short residence time ligands **12b**, **12c**, and **12f** weakened the Glu169−His264 salt bridge compared with the core scaffold in both neutral and protonated forms (Figure 4).

DISCUSSION

The relatively recent availability of high resolution X-ray structures of GPCRs has facilitated understanding of factors governing the association and dissociation of ligands. Molecular dynamics simulations have highlighted movements of the protein, which are required for ligands to enter and leave their

DOI: 10.1021/acs.jmedchem.6b00653
J. Med. Chem. 2016, 59, 6470−6479

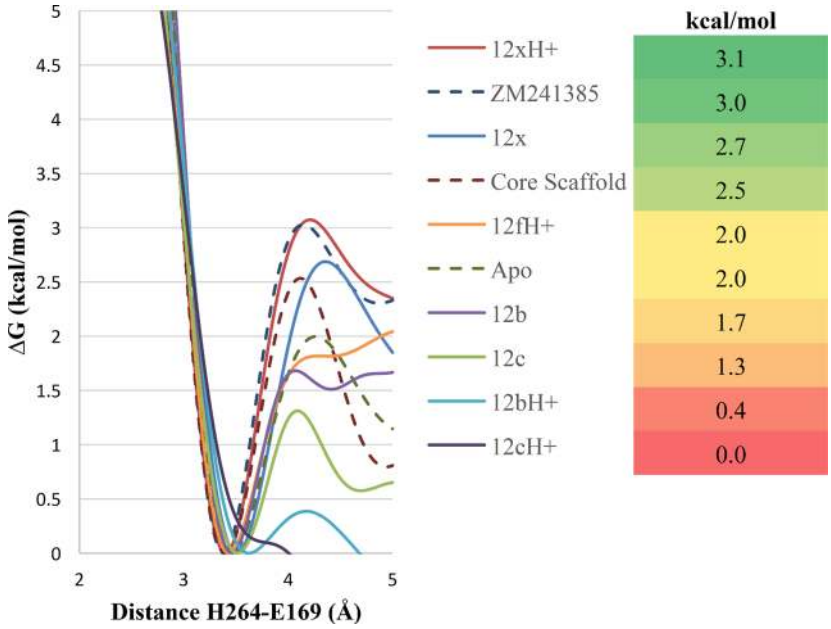

Figure 4. Evaluation of the His264−Glu169 salt bridge using metadynamics. Comparison of the predicted free energy profile for all the systems considered in function of the distance between His264 and Glu169 (see also Supporting Information Figure 1).

binding sites,[8,15] and in the case of the $A_{2A}R$ the involvement of specific residues in the dissociation of ZM241385 has been confirmed by mutagenesis.[8] In the present study, ZM241385 and a series of derivatives with a range of residence times at the $A_{2A}R$ of approximately 100-fold were selected for detailed structural investigation. Pharmacological characterization of the $A_{2A}R$, engineered to enhance thermostability and crystallization properties, demonstrates that the relative affinities and binding kinetics of the ligands are generally maintained, with a slight decrease in the binding and dissociation rate constants for the StaR, consistent with a conformationally locked form.

The near identical positions of equivalent atoms in the X-ray structures of the complexes indicate that the variations in residence time are not due to gross changes in the interactions between protein and ligand but rather are localized to areas where the ligands differ. The most pronounced differences are the interactions with His264, which is involved in a salt bridge with Glu169. This salt bridge links the second and third extracellular loops, closing off one side of the ligand binding cavity, and disrupting the salt bridge through mutagenesis of either residue is known to accelerate the dissociation of ZM241385.[8] This salt bridge has previously been observed in structures of $A_{2A}R$ with ZM241385 at pH 5[13] and pH 6.5[14] but is broken in the structure at pH 8.1,[12] presumably due to deprotonation of the histidine.

Glu169 can also directly influence the triazolotriazine core through interaction with the exocyclic amine N15 and with a water molecule, which also H-bonds to $Asn253^{6.55}$ and $Thr256^{6.58}$. This water appears to be a key structural component of the ligand costructures reported here, displaying the lowest crystallographic *B* factors of all the waters in the vicinity of the ligands. $Asn253^{6.55}$ is well established as a primary determinant of ligand binding to the $A_{2A}R$,[14] and the importance of $Thr256^{6.58}$ has been demonstrated through mutagenesis.[8]

Disruption of the salt bridge through mutagenesis increased the dissociation rate of the longest residence time ligand, **12x**, while having little effect on the short residence time ligand **12c**. It appears that, while the salt bridge is present for the longer residence time ligands and restricts their dissociation, it is readily broken for those with shorter residence times, exerting little effect on their exit from the binding site. Little effect was also observed for ZM241385, which has an intermediate residence time for the $A_{2A}R$-WT, and it is possible that, over the time scale measured by this experiment, ZM241385 was fully exchanged even without disruption of the salt bridge.

These observations suggest that the longest residence time ligand **12x** is specifically stabilizing the salt bridge. This is consistent with the structural data, where **12x** forms a π-stack interaction with the ring of His264. The distance between the difluorophenyl and the histidine rings is close to ideal for this arrangement,[16] and related compounds, with a variety of substituents on the phenyl ring, generally display long relative residence times.[9] For ZM241385, the edge to face interaction of the phenyl group with His264 is also a stabilizing interaction. The three shorter residence time ligands (**12b**, **12c**, and **12f**) however do not form stabilizing interactions with the histidine. Differences between the effects of each ligand on the stability of the salt bridge were also probed by metadynamics simulations. Enhanced sampling molecular dynamics was previously used to examine the pathway of ZM241385 dissociation from $A_{2A}R$.[8] In this work, the metadynamics approach[17] is used to estimate, with a history-dependent biased potential,[10] the energy required to break the salt bridge. The metadynamics simulations showed that ZM241385 and **12x** stabilize the His−Glu interaction, while **12b**, **12c**, and **12f** have no stabilizing effect and are possibly destabilizing the salt bridge.

It should be noted that the interaction with the salt bridge is only one of several contacts these ligands make with $A_{2A}R$. The ligand with the shortest residence time, **12f**, has an affinity of 31 ± 6 nM for the wild-type receptor, probably largely determined by the furan substituted triazolotriazine core. This is consistent with the previously reported structure of ZM241385 with $A_{2A}R$ at pH 8.1,[12] where the salt bridge is not present, but the triazolotriazine core is positioned roughly as in the structures where the salt bridge is present. The salt bridge thus, appears to

DOI: 10.1021/acs.jmedchem.6b00653
J. Med. Chem. 2016, 59, 6470−6479

represent a gate governing the dissociation of ligands from the orthosteric pocket. When it is open (Figure 3B), the ligand may exit the orthosteric site, but when closed it represents a potentially important kinetic bottleneck for ligand dissociation. Interestingly, a salt bridge is seen to form in a nearby but not equivalent site in the β2 receptor upon ligand binding, although its role has been attributed to receptor activation rather than modulation of ligand dissociation.[18]

This study of $A_{2A}R$ and five related triazolotriazine ligands demonstrates how the stability of the salt bridge on the extracellular side of the receptor can vary depending on the ligand complexed with the receptor. The nature of the ligand thus modulates the stability of the salt bridge, which controls the dissociation rate of the ligand. This illustrates a means by which, through detailed examination of protein structures and design of ligands to alter the stability of a key feature within the receptor, medicinal chemists can optimize receptor residence times.

EXPERIMENTAL SECTION

Chemicals and Reagents. [^{3}H]-ZM241385 (specific activity 49 Ci mmol^{-1}) was purchased from ARC Inc. (St. Louis, MO, USA). ZM241385 was a gift from Dr. S. M. Poucher (Astra Zeneca, Macclesfield, UK). Ligands **12x**, **12c**, **12b**, and **12f** were prepared in house following the synthetic route described in Guo et al.[9] Analytical purity was determined as described previously,[9] and all compounds were at least 95% pure. Adenosine deaminase (ADA) was purchased from Boehringer Mannheim (Manheim, Germany). Bicinchoninic acid and BCA protein assay reagent were obtained from Pierce Chemical Company (Rockford, IL, USA). All other chemicals were of analytical grade and obtained from standard commercial sources.

The A_{2A}-StaR2-bRIL Construct. The A_{2A}-StaR2-bRIL construct consists of eight thermostabilizing mutations, A54L$^{2.52}$, T88A$^{3.36}$, R107A$^{3.55}$, K122A$^{4.43}$, L202A$^{5.63}$, L235A$^{6.37}$, V239A$^{6.41}$, and S277A$^{7.42}$, and another mutation N154A to remove a glycosylation site. A FLAG tag has been added to the N-terminus of $A_{2A}R$. After K315, residues corresponding to $A_{2A}R$ have been replaced by three alanines and ten histidines. Apocytochrome b 562 RIL (bRIL)[13] is inserted into the third intracellular loop (ICL3) between residues L208 and E219.

Site Directed Mutagenesis of $A_{2A}R$. Site-directed mutants were constructed by PCR mutagenesis using pcDNA3.1−h$A_{2A}R$ with N-terminal HA and FLAG tags and C-terminal His tag as a template. The mutant E169Q was generated by Baseclear (Leiden, the Netherlands), and the H264A mutant was created in house as follows. Mutant primers for directional PCR product cloning were designed using the online Quickchange primer design program (Agilent Technologies), and primers were obtained from Eurogentec (Maastricht, the Netherland). All DNA sequences were verified by Sanger sequencing at LGTC (Leiden, the Netherlands).

Cell Culture, Transfection, and Membrane Preparation. We followed procedures as described previously.[19] Briefly, human embryonic kidney (HEK) 293 cells were grown as monolayers in Dulbecco's modified Eagle's medium (DMEM) supplemented with stable glutamine, 10% newborn calf serum, streptomycin, and penicillin at 37 °C in a moist, 7% CO_2 atmosphere. The cells were transfected with plasmid DNA using a calcium phosphate method followed by 48 h incubation before membrane preparation. Cells were detached from the plates by scraping into PBS. Cells were collected and centrifuged at 700g (3000 rpm) for 5 min. Pellets from 10 plates (10 cm diameter) were pooled and resuspended in 8 mL of ice cold buffer containing 50 mM Tris-HCl, pH 7.4. Cell suspension was homogenized with an UltraThurrax homogenizer (Heidolph Instruments, Schwabach, Germany). Cell suspension was centrifuged at 100 000g (31000 rpm) in a Beckman Optima LE-80K ultracentrifuge at 4 °C for 20 min. The pellet was resuspended in 4 mL of Tris buffer, and the homogenization and centrifugation step was repeated. After this, Tris buffer (2 mL) was used to resuspend the pellet, and ADA was added (0.8 IU/mL) to break down endogenous adenosine. Membranes were stored in 200 μL aliquots at −80 °C. Membrane protein concentrations were measured using the BCA (bicinchoninic acid) method.[20]

Radioligand Displacement Assay. Radioligand displacement experiments were performed with membranes of HEK293 cells expressing the A_{2A}-StaR2-bRIL using 11 concentrations of unlabeled ligand (from 10^{-12} to 10^{-6} M) in the presence of 3.5 nM [^{3}H]-ZM241385 at 4 °C. Membrane aliquots containing 2.5 μg of protein were incubated in a total volume of 100 μL of assay buffer (50 mM Tris-HCl, pH 7.4, supplemented with 5 mM $MgCl_2$ and 0.1% CHAPS). Nonspecific binding was determined in the presence of 10 μM ZM241385 and represented less than 10% of the total binding. [^{3}H]-ZM241385 did not bind specifically to membranes prepared from parental HEK293 cells. Incubations were terminated by rapid vacuum filtration to separate the bound and free radioligand through 96-well GF/B filter plates using a PerkinElmer FilterMate-harvester (PerkinElmer, Groningen, Netherlands) after 2 h incubation. Filters were subsequently washed three times with 2 mL of ice-cold buffer (50 mM Tris-HCl, pH 7.4, supplemented with 5 mM $MgCl_2$). The filter-bound radioactivity was determined by scintillation spectrometry using a P-E 1450 Microbeta Wallac Trilux scintillation counter (PerkinElmer, Groningen, Netherlands).

Association experiments were performed by incubating membrane aliquots of HEK293 cells expressing the A_{2A}-StaR2-bRIL (2.5 μg) in a total volume of 100 μL of assay buffer at 4 °C with 3.5 nM [^{3}H]-ZM241385. The amount of radioligand bound to the receptor was measured at different time intervals during incubation for 4 h. Dissociation experiments of [^{3}H]-ZM241385 on the wild-type or A_{2A}-StaR2-bRIL were performed by preincubating membrane suspension (2.5−5 μg) with [^{3}H]-ZM241385 in 100 μL of assay buffer at 4 °C for 2 h. After the preincubation, the dissociation was initiated by addition of 1 μM of unlabeled ZM241385 in 5 μL. The amount of radioligand still bound to the receptor was measured at various time intervals for a total duration of 2−6 h at 4 °C to ensure that [^{3}H]-ZM241385 was fully dissociated from the wild-type $A_{2A}R$ or A_{2A}-StaR2-bRIL receptors. Incubations were terminated and samples were obtained as described under radioligand displacement assays.

The binding kinetics of unlabeled ligands were determined at 4 °C using the competition association assay as described by Guo et al.[21] The competition association assay was initiated by adding membrane aliquots (2.5 μg/well) at different time points for a total of 240 min to a total volume of 100 μL of assay buffer at 4 °C with 3.5 nM [^{3}H]-ZM241385 in the absence or presence of competing ligand at their respective IC_{50} values. Incubations were terminated and samples were obtained as described for radioligand displacement assays.

For radioligand wash-out experiments, membranes of HEK293 cells expressing the $A_{2A}R$ were pretreated with 1 μM **12x**, **12c**, or ZM241385 at 25 °C for 1 h. Subsequently, the pretreated membrane was washed with 1 mL assay buffer and then incubated for 10 min at 25 °C. The unbound ligands were discarded after centrifugation at 16000g for 2 min at 4 °C. The pellet was resuspended in 1 mL of assay buffer, and the washing and centrifugation step was repeated three times. After this the membrane preparations were incubated with 2.5 nM [^{3}H]-ZM241385 for 30 min. Incubations were terminated and samples were obtained as described for radioligand displacement assays.

Data Analysis. All experimental data were analyzed by using GraphPad Prism 6.0 (GraphPad Software Inc., San Diego, CA). Values obtained are mean ± SEM of at least three independent experiments performed in duplicate. IC_{50} values obtained from displacement binding data were converted into K_i values using the Cheng−Prusoff equation.[22] Dissociation data were fitted using a model of one-phase exponential decay to obtain k_{off}. Association data were fitted using a model of one-phase exponential association. Values for k_{on} were obtained by converting k_{obs} values using the following equation:

$$k_{on} = (k_{obs} - k_{off})/[\text{radioligand}]$$

where k_{off} values were assessed from independent dissociation experiments. The residence time (RT) was calculated using RT =

DOI: 10.1021/acs.jmedchem.6b00653
J. Med. Chem. 2016, 59, 6470−6479

$1/k_{off}$.[23] Association and dissociation rates for unlabeled ligands (**12x**, **12c**, **12b**, and **12f**) at the membranes of HEK293 cells expressing the A_{2A}-StaR2-bRIL were calculated by fitting the data in the competition association model using kinetics of competitive binding:[24]

$$K_A = k_1[L] \times 10^{-9} + k_2$$

$$K_B = k_3[I] \times 10^{-9} + k_4$$

$$S = \sqrt{(K_A - K_B)^2 + 4k_1k_3LI \times 10^{-18}}$$

$$K_F = 0.5(K_A + K_B + S)$$

$$K_S = 0.5(K_A + K_B - S)$$

$$Q = \frac{B_{max}k_1L \times 10^{-9}}{K_F - K_S}$$

$$Y = Q\left(\frac{k_4(K_F - K_S)}{K_FK_S} + \frac{k_4 - K_F}{K_F}e^{(-K_FX)} - \frac{k_4 - K_S}{K_S}e^{(-K_SX)}\right)$$

where X is the time (min), Y is the specific [^{3}H]-ZM241385 binding (DPM), k_1 and k_2 are the k_{on} ($M^{-1}\cdot min^{-1}$) and k_{off} (min^{-1}), respectively, of [^{3}H]-ZM241385 at the membrane of HEK293 cells expressing the A_{2A}-StaR2-bRIL determined from radioligand association and dissociation assays, L is the concentration of [^{3}H]-ZM241385 used (nM), B_{max} is the total binding (DPM), and I is the concentration unlabeled ligand (nM). Fixing these parameters allows the following parameters to be calculated: k_3, which is the k_{on} value ($M^{-1}\cdot min^{-1}$) of the unlabeled ligand, and k_4, which is the k_{off} value (min^{-1}) of the unlabeled ligand. Statistical analyses were performed using one-way ANOVA with Dunnett's test (*$P < 0.05$, **$P < 0.01$, ***$P < 0.001$).

Structural Biology. The A_{2A}-StaR2-bRIL was expressed using the baculovirus system. Tni PRO cells were grown in suspension in flasks up to a maximum volume of 500 mL in 2 L roller bottles at 27 °C with shaking. Cells were grown in ESF921 (Expression Systems) medium supplemented with 5% (v/v) FBS and 1% (v/v) penicillin/streptomycin. Cells at a density of 2.6×10^6 cells/mL were infected with recombinant virus at an approximate multiplicity of infection of 1. Cells were harvested by centrifugation 48 h postinfection.

Membranes were prepared from a pellet of cells from a 2 L culture resuspended in 40 mM Tris−HCl, pH 7.6, 1 mM EDTA, and Complete EDTA-free protease inhibitor cocktail tablets (Roche). Cells were disrupted through a microfluidizer (processor M-110L Pneumatic, Microfluidics) cooled with ice (lysis pressure ∼15 000 psi), and membranes were pelleted by centrifugation at 200 000*g* for 50 min. Membranes were washed with 40 mM Tris−HCl, pH 7.6, 1 M NaCl, and Complete EDTA-free protease inhibitor cocktail tablets and centrifuged at 200 000*g* for 50 min. After removal of the supernatant, membranes were resuspended in 50 mL of 40 mM Tris−HCl, pH 7.6, with Complete EDTA-free protease inhibitor cocktail tablets and frozen at −80 °C.

Membranes were resuspended in a total volume of 150 mL with 40 mM Tris−HCl, pH 7.6, Complete EDTA-free protease inhibitor cocktail tablets (Roche), and 5 μM of the appropriate ligand and incubated for 1 h at room temperature. Membranes were then solubilized by addition of 1.5% *n*-decyl-β-D-maltopyranoside (DM) for 1 h at 4 °C followed by centrifugation at 145 000*g* for 60 min to remove insoluble material.

All protein purification steps were carried out at 4 °C. The solubilized material was applied to a 5 mL Ni-NTA (nickel−nitrilotriacetic acid) superflow cartridge (Qiagen) pre-equilibrated in 40 mM Tris, pH 7.4, 200 mM NaCl, 0.15% DM, and 5 μM ligand. The column was washed with 25 column volumes of buffer 40 mM Tris, pH 7.4, 200 mM NaCl, 0.15% DM, 70 mM imidazole, and 5 μM ligand, and then the protein was eluted with 40 mM Tris, pH 7.4, 200 mM NaCl, 0.15% DM, 280 mM imidazole, and 5 μM ligand.

Fractions were collected and analyzed by SDS PAGE gel. Fractions containing A_{2A}-StaR2-bRIL were pooled and concentrated using an Amicon Ultra Ultracell 50K ultrafiltration membrane to a final volume of ∼800 μL. The protein sample was applied to a 10/30 S200 size exclusion column (GE Healthcare) pre-equilibrated with 40 mM Tris pH 7.4, 200 mM NaCl, 0.15% DM, and 5 μM ligand and eluted at 0.5 mL/min. Column fractions were collected and analyzed by SDS PAGE gel, and fractions containing the protein were pooled and concentrated to ∼30 mg/mL. Protein concentrations were measured at 280 nm on a Nanodrop 8000 UV−vis spectrophotometer (Thermo Scientific) using the protein's extinction coefficient of 58745 M^{-1} cm^{-1}.

The A_{2A}-StaR2-bRIL was crystallized in lipidic cubic phase at 20 °C. Protein was concentrated to 25−35 mg mL^{-1} except with **12c** where it was concentrated to 57 mg mL^{-1}. Concentrated protein was mixed with monoolein (Nu-Chek) supplemented with 10% (w/w) cholesterol (Sigma-Aldrich) and 5 μM ligand using the twin-syringe method.[25] The final protein/lipid ratio was 1:1.5 (w/w). Boluses of 40−60 nL were dispensed onto 96-well laminex glass base (Molecular Dimensions Ltd) using a Mosquito LCP crystallization robot (TTP Labtech) and overlaid with 0.75 μL of precipitant solution. With ZM241385 and **12x**, crystals were obtained in 0.1 M MES, pH 5.5, 0.2 M K/Na tartrate, 27.5−40% PEG400, and 0.5−1% (v/v) (±)-2-methyl-2,4-pentanediol. With **12b** and **12c**, crystals were obtained in 0.1 M trisodium citrate, pH 5.3−5.4, 0.05 M sodium thiocyanate, 29−32% PEG400, and 2% (v/v) 2,5-hexanediol. Crystals with **12f** were obtained in 0.1 M MES, pH 5.5, 0.2 M K/Na tartrate, 33.5% PEG400, and 0.5% (v/v) 1,2,3-heptanetriol. Crystals measuring 60−80 μm long appeared within a few days and were harvested within 2 weeks by snap-freezing in liquid nitrogen using a mounted litholoop (Molecular Dimensions Ltd.).

X-ray diffraction data were measured with crystals frozen in liquid nitrogen on a Pilatus 6 M detector at Diamond Light Source beamline I24 except for **12x** where data were collected at I04. Crystals were exposed with a 10 μm × 10 μm mini-beam at an X-ray wavelength of 0.9686 Å (ZM241385, **12c**, **12f**), 0.9698 Å (**12b**), and 0.9795 Å (**12x**) using 0.2° (ZM241385), 0.25° (**12c**), and 0.5° (**12x**, **12b**, **12c**) oscillation per frame. Radiation damage meant multiple crystals were needed to merge into a complete data set except for the **12c** complex where a complete data set was obtained from a single crystal. Diffraction images were integrated using XDS,[26] merged, and scaled using AIMLESS.[27]

Structures were solved by molecular replacement using the A_{2A}-bRIL fusion (PDB accession 4EIY) with the program Phaser.[28] Refinements were done using the Phenix package[29] followed by manual rebuilding and model improvement in Coot[30] using both $|2F_o| - |F_c|$ and $|F_o| - |F_c|$ maps. Quality of structures was assessed using Molprobity.[31]

Molecular Dynamics and Metadynamics Simulations. The fusion protein bRIL was removed from the A_{2A}-StaR2-bRIL crystal structure in complex with the ligand **12x**, and the missing loop from residue 209 to 218 was modeled using Prime[32] (Prime, version 3.9, Schrödinger, LLC, New York, NY, 2015). The receptor was prepared with the Protein Preparation Wizard in Maestro (Maestro, version 10.1, Schrödinger, LLC, New York, NY, 2015): the H-bond network was optimized through an exhaustive sampling of hydroxyl and thiol moieties, tautomeric and ionic state of His, and 180° rotations of the terminal dihedral angle of amide groups of Asp and Gln. His264 was considered to be protonated. The crystal structures of A_{2A}-StaR2-bRIL in complex with ZM241385, **12c**, and **12b** were superimposed on the A_{2A}-StaR2-bRIL−**12x** complex. Both neutral and positively charged states of **12x**, **12c**, and **12b** were analyzed, while **12f** was only considered to be protonated (Figure 1). In addition the core scaffold, common among all the ligands considered, was included in the analysis (Figure 1), and also an apo state of the receptor generated by removing **12x** from the crystal structure.

Each ligand−receptor complex was equilibrated using the following molecular dynamics protocol. The AMBER99SB force field (ff) parameters[33] were used for the protein and the GAFF ff[34] for the ligands using AM1-BCC partial charges.[35] The system was embedded in a triclinic box including an equilibrated membrane consisting of 256 DMPC (1,2-dimyristoyl-*sn*-glycero-3-phosphocholine) lipids[36] and 24513 waters using g_membed[37] in Gromacs. The SPC water model was used, and ions were added to neutralize the system (final

DOI: 10.1021/acs.jmedchem.6b00653
J. Med. Chem. 2016, 59, 6470−6479

concentration 0.01 M). An energy minimization protocol based on 1000 steps steepest-descent algorithm has been applied to the system. The membrane was equilibrated using 0.5 ns MD simulation with a time step of 2.5 fs, using LINCS on all bonds and keeping the protein and ligand restrained applying a force of 100 kJ mol^{-1} nm^{-1}. Lennard-Jones and Coulomb interactions were treated with a cutoff of 1.069 nm with particle-mesh Ewald electrostatics (PME).[38] The MD was executed in the NPT ensemble using v-rescale[39] (tau_t = 0.5 ps) for the temperature coupling to maintain the temperature of 298 K and using Parrinello−Rahman[40] (tau_p = 10.0 ps) for the semi-isotropic pressure coupling to maintain the pressure of 1.013 bar. Without applying any positional restraints, the system was minimized for 200 steps using the steepest-descent algorithm and equilibrated using MD with the same settings described above, but with a time step of 0.2 fs and increasing the temperature from 29.8 to 298 K in 10 steps (9 steps of 30 ps and the last one of 300 ps). Using the same protocol, the system was equilibrated for 3 ns at 298 K and then subjected to 10 ns metadynamics.[10] For the metadynamics, two collective variables (CVs) were included to evaluate the state of the Glu169−His264 salt bridge: (I) the distance between ε N of His264 and δ C of Glu169; (II) His264 dihedral angle defined by its carbonyl carbon, Cα, Cβ, and Cγ atoms. In the well-tempered metadynamics simulations,[41] a history dependent bias composed of intermittently added Gaussian functions was added to the potential. The bias was updated by adding Gaussian contributions with a total height of

$$W = W_0 \exp\left(-\frac{V_t(s, z)}{fT}\right) \quad (3)$$

where W_0 is the initial Gaussian height, T is the simulation temperature, f is the bias factor, and $V_t(s,z)$ is the bias potential at time t for the values s and z of the CVs. For the metadynamics, the following parameters were applied: simulated temperature 298 K, bias factor 6, and initial energy bias Gaussian height of 0.3 kcal/mol with a deposition frequency of 0.5 ps. The width of the Gaussians was 0.4 Å for the Glu169−His264 distance CV and 0.3 rad for the His264 torsional angle. The obtained free energy landscape for all the systems considered (Supporting Information Figure 1) was analyzed to estimate the energy barrier required to break the salt bridge as described by the distance between Glu169 and His264 (Figure 3B).

■ ASSOCIATED CONTENT

Supporting Information

The Supporting Information is available free of charge on the ACS Publications website at DOI: 10.1021/acs.jmedchem.6b00653.

Free energy landscape plots from the metadynamics simulations for each ligand (PDF)

Accession Codes

5IU4, A_{2A}-StaR2-bRIL in complex with ZM241385; 5IU7, A_{2A}-StaR2-bRIL in complex with **12c**; 5IU8, A_{2A}-StaR2-bRIL in complex with **12f**; 5IUA, A_{2A}-StaR2-bRIL in complex with **12b**; 5IUB, A_{2A}-StaR2-bRIL in complex with **12x**. Authors will release the atomic coordinates upon article publication.

■ AUTHOR INFORMATION

Corresponding Author

*Dr. Robert M. Cooke. E-mail: Rob.cooke@heptares.com. Tel: +44 1707 358639.

Present Addresses

Dr. Dong Guo: Jiangsu Key Laboratory of New Drug Research and Clinical Pharmacy, Xuzhou Medical University, Tongshan Road 209, 221004 Xuzhou, Jiangsu, China.

Dr Robert K. Y. Cheng: leadXpro AG, PARK InnovAARE, 5234 Villigen, Switzerland.

Author Contributions

#E.S., D.G., and R.K.Y.C. contributed equally to this work. E.S. expressed and purified the A_{2A}-StaR2-bRIL protein with compounds. D.G. characterized the kinetics of compound binding. R.K.Y.C. crystallized the protein complexes, collected X-ray data, and solved and refined structures. A.S.D. and J.C.E. devised and implemented the strategy of transferring StaR mutations to the A_{2A}-bRIL construct. A.B. and F.D. performed the metadynamics analysis of complexes. L.H.H., A.P.I., J.C.E., A.S.D., F.H.M., and R.M.C. assisted with design of experiments, project management, and interpretation of results. All authors contributed to writing the manuscript.

Notes

The authors declare the following competing financial interest(s): E.S., A.B., F.D., A.S.D., J.C.E., F.H.M., and R.M.C. are employees of Heptares Therapeutics Ltd. R.K.Y.C. was an employee of Heptares Therapeutics Ltd when the work was performed.

■ ACKNOWLEDGMENTS

The authors thank Ali Jazayeri for molecular biology support for generation of the A_{2A}-StaR2-bRIL construct and Cédric Fiez-Vandal for assistance with expression and purification. The research leading to these results has received support from the Innovative Medicines Initiative Joint Undertaking under K4DD (www.k4dd.eu), Grant Agreement No. 115366, resources of which are composed of financial contribution from the European Union's Seventh Framework Programme (FP7/2007−2013) and EFPIA companies' in kind contribution. More info see www.imi.europa.eu.

■ ABBREVIATIONS USED

A_{2A}R, A_{2A} adenosine receptor; ADHD, attention deficit hyperactivity disorder; bRIL, thermostabilized apocytochrome b; StaR, stabilized receptor; T4L, bacteriophage T4 lysozyme

■ REFERENCES

(1) Overington, J. P.; Al-Lazikani, B.; Hopkins, A. L. How many drug targets are there? *Nat. Rev. Drug Discovery* **2006**, *5*, 993−996.

(2) Cooke, R. M.; Brown, A. J.; Marshall, F. H.; Mason, J. S. Structures of G protein-coupled receptors reveal new opportunities for drug discovery. *Drug Discovery Today* **2015**, *20*, 1355−1364.

(3) Copeland, R. A.; Pompliano, D. L.; Meek, T. D. Drug-target residence time and its implications for lead optimization. *Nat. Rev. Drug Discovery* **2006**, *5*, 730−739.

(4) Lu, H.; Tonge, P. J. Drug-target residence time: critical information for lead optimization. *Curr. Opin. Chem. Biol.* **2010**, *14*, 467−474.

(5) Pan, A. C.; Borhani, D. W.; Dror, R. O.; Shaw, D. E. Molecular determinants of drug-receptor binding kinetics. *Drug Discovery Today* **2013**, *18*, 667−673.

(6) Pinna, A. Adenosine A2A receptor antagonists in Parkinson's disease: progress in clinical trials from the newly approved istradefylline to drugs in early development and those already discontinued. *CNS Drugs* **2014**, *28*, 455−474.

(7) Leone, R. D.; Lo, Y. C.; Powell, J. D. A2aR antagonists: Next generation checkpoint blockade for cancer immunotherapy. *Comput. Struct. Biotechnol. J.* **2015**, *13*, 265−272.

(8) Guo, D.; Pan, A. C.; Dror, R. O.; Mocking, T.; Liu, R.; Heitman, L. H.; Shaw, D. E.; IJzerman, A. P. Molecular basis of ligand dissociation from the adenosine A_{2A} receptor. *Mol. Pharmacol.* **2016**, *89*, 485−491.

(9) Guo, D.; Xia, L.; van Veldhoven, J. P.; Hazeu, M.; Mocking, T.; Brussee, J.; IJzerman, A. P.; Heitman, L. H. Binding kinetics of

DOI: 10.1021/acs.jmedchem.6b00653
J. Med. Chem. 2016, 59, 6470−6479

ZM241385 derivatives at the human adenosine A2A receptor. *ChemMedChem* **2014**, *9*, 752−761.
(10) Laio, A.; Parrinello, M. Escaping free energy minima. *Proc. Natl. Acad. Sci. U. S. A.* **2002**, *99*, 12562−12566.
(11) Ballesteros, J.; Weinstein, H. Integrated methods for the construction of three-dimensional models and computational probing of structure-function relations in G protein-coupled receptors. *Methods Neurosci.* **1995**, *25*, 366−428.
(12) Dore, A. S.; Robertson, N.; Errey, J. C.; Ng, I.; Hollenstein, K.; Tehan, B.; Hurrell, E.; Bennett, K.; Congreve, M.; Magnani, F.; Tate, C. G.; Weir, M.; Marshall, F. H. Structure of the adenosine A_{2A} receptor in complex with ZM241385 and the xanthines XAC and caffeine. *Structure* **2011**, *19*, 1283−1293.
(13) Liu, W.; Chun, E.; Thompson, A. A.; Chubukov, P.; Xu, F.; Katritch, V.; Han, G. W.; Roth, C. B.; Heitman, L. H.; IJzerman, A. P.; Cherezov, V.; Stevens, R. C. Structural basis for allosteric regulation of GPCRs by sodium ions. *Science* **2012**, *337*, 232−236.
(14) Jaakola, V. P.; Griffith, M. T.; Hanson, M. A.; Cherezov, V.; Chien, E. Y.; Lane, J. R.; IJzerman, A. P.; Stevens, R. C. The 2.6 angstrom crystal structure of a human A_{2A} adenosine receptor bound to an antagonist. *Science* **2008**, *322*, 1211−1217.
(15) Kruse, A. C.; Hu, J.; Pan, A. C.; Arlow, D. H.; Rosenbaum, D. M.; Rosemond, E.; Green, H. F.; Liu, T.; Chae, P. S.; Dror, R. O.; Shaw, D. E.; Weis, W. I.; Wess, J.; Kobilka, B. K. Structure and dynamics of the M3 muscarinic acetylcholine receptor. *Nature* **2012**, *482*, 552−556.
(16) Bissantz, C.; Kuhn, B.; Stahl, M. Medicinal chemist's guide to molecular interactions. *J. Med. Chem.* **2010**, *53*, 5061−5084.
(17) Schneider, S.; Provasi, D.; Filizola, M. The dynamic process of drug-GPCR binding at either orthosteric or allosteric sites evaluated by metadynamics. In *G Protein-Coupled Receptors in Drug Discovery*; Filizola, M., Ed.; Springer: New York, 2015; pp 277−294.
(18) Bokoch, M. P.; Zou, Y.; Rasmussen, S. G. F.; Liu, C. W.; Nygaard, R.; Rosenbaum, D. M.; Fung, J. J.; Choi, H.-J.; Thian, F. S.; Kobilka, T. S.; Puglisi, J. D.; Weis, W. I.; Pardo, L.; Prosser, R. S.; Mueller, L.; Kobilka, B. K. Ligand-specific regulation of the extracellular surface of a G protein coupled receptor. *Nature* **2010**, *463*, 108−112.
(19) Lane, J. R.; Klein Herenbrink, C.; van Westen, G. J.; Spoorendonk, J. A.; Hoffmann, C.; IJzerman, A. P. A novel nonribose agonist, LUF5834, engages residues that are distinct from those of adenosine-like ligands to activate the adenosine A_{2a} receptor. *Mol. Pharmacol.* **2012**, *81*, 475−487.
(20) Smith, P. K.; Krohn, R. I.; Hermanson, G. T.; Mallia, A. K.; Gartner, F. H.; Provenzano, M. D.; Fujimoto, E. K.; Goeke, N. M.; Olson, B. J.; Klenk, D. C. Measurement of protein using bicinchoninic acid. *Anal. Biochem.* **1985**, *150*, 76−85.
(21) Guo, D.; Mulder-Krieger, T.; IJzerman, A. P.; Heitman, L. H. Functional efficacy of adenosine A_{2A} receptor agonists is positively correlated to their receptor residence time. *Br. J. Pharmacol.* **2012**, *166*, 1846−1859.
(22) Yung-Chi, C.; Prusoff, W. H. Relationship between the inhibition constant (K_I) and the concentration of inhibitor which causes 50% inhibition (I_{50}) of an enzymatic reaction. *Biochem. Pharmacol.* **1973**, *22*, 3099−3108.
(23) Copeland, R. A. Evaluation of enzyme inhibitors in drug discovery. A guide for medicinal chemists and pharmacologists. *Methods Biochem. Anal.* **2005**, *46*, 1−265.
(24) Motulsky, H. J.; Mahan, L. C. The kinetics of competitive radioligand binding predicted by the law of mass action. *Mol. Pharmacol.* **1984**, *25*, 1−9.
(25) Caffrey, M.; Cherezov, V. Crystallizing membrane proteins using lipidic cubic mesophases. *Nat. Protoc.* **2009**, *4*, 706−731.
(26) Kabsch, W. XDS. *Acta Crystallogr., Sect. D: Biol. Crystallogr.* **2010**, *66*, 125−132.
(27) Winn, M. D.; Ballard, C. C.; Cowtan, K. D.; Dodson, E. J.; Emsley, P.; Evans, P. R.; Keegan, R. M.; Krissinel, E. B.; Leslie, A. G. W.; McCoy, A.; McNicholas, S. J.; Murshudov, G. N.; Pannu, N. S.; Potterton, E. A.; Powell, H. R.; Read, R. J.; Vagin, A.; Wilson, K. S. Overview of the CCP4 suite and current developments. *Acta Crystallogr., Sect. D: Biol. Crystallogr.* **2011**, *67*, 235−242.
(28) McCoy, A. J.; Grosse-Kunstleve, R. W.; Adams, P. D.; Winn, M. D.; Storoni, L. C.; Read, R. J. Phaser crystallographic software. *J. Appl. Crystallogr.* **2007**, *40*, 658−674.
(29) Adams, P. D.; Afonine, P. V.; Bunkoczi, G.; Chen, V. B.; Davis, I. W.; Echols, N.; Headd, J. J.; Hung, L. W.; Kapral, G. J.; Grosse-Kunstleve, R. W.; McCoy, A. J.; Moriarty, N. W.; Oeffner, R.; Read, R. J.; Richardson, D. C.; Richardson, J. S.; Terwilliger, T. C.; Zwart, P. H. PHENIX: a comprehensive Python-based system for macromolecular structure solution. *Acta Crystallogr., Sect. D: Biol. Crystallogr.* **2010**, *66*, 213−221.
(30) Emsley, P.; Lohkamp, B.; Scott, W. G.; Cowtan, K. Features and development of Coot. *Acta Crystallogr., Sect. D: Biol. Crystallogr.* **2010**, *66*, 486−501.
(31) Chen, V. B.; Arendall, W. B.; Headd, J. J.; Keedy, D. A.; Immormino, R. M.; Kapral, G. J.; Murray, L. W.; Richardson, J. S.; Richardson, D. C. MolProbity: all-atom structure validation for macromolecular crystallography. *Acta Crystallogr., Sect. D: Biol. Crystallogr.* **2010**, *66*, 12−21.
(32) Jacobson, M. P.; Pincus, D. L.; Rapp, C. S.; Day, T. J.; Honig, B.; Shaw, D. E.; Friesner, R. A. A hierarchical approach to all-atom protein loop prediction. *Proteins: Struct., Funct., Genet.* **2004**, *55*, 351−367.
(33) Lindorff-Larsen, K.; Piana, S.; Palmo, K.; Maragakis, P.; Klepeis, J. L.; Dror, R. O.; Shaw, D. E. Improved side-chain torsion potentials for the Amber Ff99SB protein force field. *Proteins: Struct., Funct., Genet.* **2010**, *78*, 1950−1958.
(34) Wang, J.; Wolf, R. M.; Caldwell, J. W.; Kollman, P. A.; Case, D. A. Development and testing of a general Amber force field. *J. Comput. Chem.* **2004**, *25*, 1157−1174.
(35) Jakalian, A.; Jack, D. B.; Bayly, C. I. Fast, efficient generation of high-quality atomic charges. AM1-BCC model: II. Parameterization and validation. *J. Comput. Chem.* **2002**, *23*, 1623−1641.
(36) Jambeck, J. P.; Lyubartsev, A. P. Derivation and systematic validation of a refined all-atom force field for phosphatidylcholine lipids. *J. Phys. Chem. B* **2012**, *116*, 3164−3179.
(37) Wolf, M. G.; Hoefling, M.; Aponte-Santamaria, C.; Grubmuller, H.; Groenhof, G. G_Membed: efficient insertion of a membrane protein into an equilibrated lipid bilayer with minimal perturbation. *J. Comput. Chem.* **2010**, *31*, 2169−2174.
(38) Darden, T.; York, D.; Pedersen, L. Particle mesh Ewald: an N Log (N) method for Ewald sums in large systems. *J. Chem. Phys.* **1993**, *98*, 10089−10092.
(39) Bussi, G.; Donadio, D.; Parrinello, M. Canonical sampling through velocity rescaling. *J. Chem. Phys.* **2007**, *126*, 014101.
(40) Parrinello, M.; Rahman, A. Polymorphic transitions in single crystals: a new molecular dynamics method. *J. Appl. Phys.* **1981**, *52*, 7182−7190.
(41) Barducci, A.; Bussi, G.; Parrinello, M. Well-tempered Metadynamics: a smoothly converging and tunable free-energy method. *Phys. Rev. Lett.* **2008**, *100*, 020603.

DOI: 10.1021/acs.jmedchem.6b00653
J. Med. Chem. 2016, 59, 6470−6479